Size-Effects on the VHCF Response of Flat Metallic Specimens for Automotive Applications: Analysis of Fatigue Data with a Method Based on the Stress Gradient

ASTM INTERNATIONAL

Materials Performance and Characterization

Andrea Tridello,[1] Carlo Boursier Niutta,[2] Filippo Berto,[3] and Davide Salvatore Paolino[2]

DOI: 10.1520/MPC20220086

Size-Effects on the VHCF Response of Flat Metallic Specimens for Automotive Applications: Analysis of Fatigue Data with a Method Based on the Stress Gradient

Materials Performance and Characterization

doi:10.1520/MPC20220086 available online at www.astm.org

Andrea Tridello,[1] Carlo Boursier Niutta,[2] Filippo Berto,[3] and Davide Salvatore Paolino[2]

Size-Effects on the VHCF Response of Flat Metallic Specimens for Automotive Applications: Analysis of Fatigue Data with a Method Based on the Stress Gradient

Reference

A. Tridello, C. Boursier Niutta, F. Berto, and D. S. Paolino, "Size-Effects on the VHCF Response of Flat Metallic Specimens for Automotive Applications: Analysis of Fatigue Data with a Method Based on the Stress Gradient," *Materials Performance and Characterization* https://doi.org/10.1520/MPC20220086

ABSTRACT

The design against fatigue failures at very high number of cycles (VHCF) is fundamental to guarantee the integrity of components used in structural applications (aerospace, energy production, automotive). Experimental tests to assess the VHCF response of materials are generally carried out on small specimens with sizes that are significantly different from those of the components to be designed. Size-effect, which is widely known to affect the VHCF response, must therefore be properly modeled and accounted when components are designed to ensure their structural integrity. Size-effects in VHCF have been generally investigated by testing specimens with circular cross-sections and modeled by considering the probabilistic increment of the defect size with the loaded volume. In the present paper, ultrasonic fatigue tests have been carried out on hourglass flat specimens and larger dog-bone flat specimens to investigate size-effects. One aluminum alloy and four steels used for automotive applications have been tested. The experimental results have been analyzed with an innovative statistical model based on the weakest-link principle and on the stress gradient within the specimens, which does not require the size of the defect at the origin of the fatigue failure, generally not available if the specimen fails from the surface. Size-effects were found to significantly influence the VHCF response of the investigated materials, further confirming that it is strongly material dependent, even for flat specimens. A general rule for size-effect in VHCF of flat specimens was not found, proving that it must be properly experimentally verified and safely accounted when designing large components against VHCF failure.

Manuscript received September 30, 2022; accepted for publication January 18, 2023; published online March 3, 2023.

[1] Department of Mechanical and Aerospace Engineering, Politecnico di Torino, Corso Duca Degli Abruzzi, 24, 10129 Turin, Italy (Corresponding author), e-mail: andrea.tridello@polito.it, https://orcid.org/0000-0003-3007-3377

[2] Department of Mechanical and Aerospace Engineering, Politecnico di Torino, Corso Duca Degli Abruzzi, 24, 10129 Turin, Italy, https://orcid.org/0000-0002-7894-4752 (C.B.N.), https://orcid.org/0000-0002-4231-4580 (D.S.P.)

[3] Department of Chemical Engineering Materials Environment, SAPIENZA - UNIVERSITÁ DI ROMA, Via Eudossiana, 18, 00184 Roma, Italy, https://orcid.org/0000-0001-9676-9970

Keywords

very high cycle fatigue, size-effect, specimen size, stress gradient, flat specimen, automotive industry

Introduction

The design against fatigue failures at very high number of cycles (VHCF) is fundamental to guarantee the integrity of components used in several structural applications (aerospace, energy production, automotive), with required fatigue life that has significantly increased in the last decades.[1–3] Particular attention has been devoted in the literature[4,5] to the VHCF response of materials used for automotive applications. Experimental tests to assess the VHCF response of automotive materials are generally carried out on small specimens with sizes significantly different from those of the components to be designed. However, it is widely known in the literature that the size-effect strongly affects the VHCF response of materials and, therefore, it must be properly modeled when designing automotive components employed for structural applications.

Size-effects in VHCF have been mainly investigated by testing specimens with circular cross-sections. However, in many automotive applications, components are cut from flat plates with small thicknesses. Experimental results in Fitzka et al.[6] have shown that the size-effects can also be large for flat specimens. Size-effects in VHCF are moreover generally modeled by considering the statistical increment of the probability of large defects with the material volume.[7–9] With this approach, the distribution of the defect size should be reliably estimated, generally by analyzing the defects from which failure originated on the fracture surfaces. However, according to Tridello, Paolino, and Rossetto,[10,11] the analysis of size-effects by only considering the distribution of the defect size and its increment with the material volume may not be effective because the stress gradient and the stress distribution within the component also play a fundamental role. Other approaches,[12] based on geometric parameters like the specimen diameter, have been proven effective for specimens, but can be hardly applied for components with complex shapes.

In this work, size-effects on the VHCF response of flat specimens have been experimentally investigated. Ultrasonic fully reversed tension-compression tests have been carried out on hourglass specimens and on dog-bone specimens with larger loaded volumes. An aluminum alloy, as well as four steels used in automotive applications and cut from flat plates with thicknesses up to 6 mm, have been tested. The experimental data have been finally analyzed with a model proposed by the authors and based on the distribution of stress amplitude within the part in order to model the influence of the stress gradient on the crack nucleation process.

Materials and Methods

In this section, the experimental activity is described. In the section "Experimental Material," the tested materials are detailed. In the section "Specimen Geometry," the procedure followed for designing hourglass and dog-bone specimens is reported. In the section "Ultrasonic Fatigue Testing Configuration," the configuration for ultrasonic fatigue tests on flat specimens is described; whereas, in Section "Statistical Model for Size-Effect in VHCF," the developed statistical model is addressed. All the experimental tests have been carried out within a European research project.

EXPERIMENTAL MATERIAL

Experimental tests have been carried out on flat specimens made of aluminum and steel alloys used in the automotive industry. The following materials have been tested:

1. AA6082 aluminum alloy, commonly used for stamping in Europe, is characterized by good mechanical properties, good formability and corrosion resistance. The tested AA6082 alloy has been provided in the T6 heat treatment, i.e., solution heat-treated and artificially aged.
2. HR CP800 SF (stretch flangeability) is a complex phase steel. Its microstructure is composed of a bainitic and ferritic matrix with martensite/austenite islands, showing a very good SF behavior.[13]

TABLE 1
Tested material and nominal mechanical properties provided by the material supplier

Material	Plate Thicknesses	Tensile Strength, MPa	Elongation to Failure
AA6082	2 and 5 mm	330 MPa	>9 %
HR CP800	3.4 mm	~800 MPa	>(10 %)
HR CP980 SF	3.5 mm	~980 MPa	>8 %
410S	3.8 mm	>900 MPa	>8 %
22MnB5	6 mm	~1,600 MPa	~7 %

3. HR CP980 SF is a complex phase steel. The microstructure is complex and composed of a matrix of tempered martensite and ferrite, combined with upper bainite, and retained austenite islands.
4. The alloy 410S is obtained by reducing the carbon content of the 410 martensitic stainless steel and by adding Nb or Ti, characterized by good corrosion resistance. The tested material has been provided after heat treatment of austenitization, 950°C for 9 min, and quenching.
5. 22MnB5 is a boron hardenable steel, characterized by high mechanical properties after quenching and used in different automotive components.[14]

The specimens have been cut from rectangular plates, whose thicknesses and indicative mechanical properties (tensile strength and elongation to failure) are reported in Table 1. The mechanical properties have been retrieved from the literature or from the websites of the material supplier.

According to Table 1, AA6082 plates with two thicknesses (2 mm and 5 mm) have been provided, whereas plates with a unique thickness were available for the tested steels. The specimens have been cut from the rectangular plates with a waterjet (AA6082, HRCP800) or laser cutting process (HRCP980, AISI 410S, 22MnB5).

SPECIMEN GEOMETRY

In order to investigate size-effects on flat specimens, two specimen geometries, hourglass and dog-bone, have been tested. The objective is to investigate the influence of the specimen size by increasing the loaded volume. In the following, the loaded volume has been assumed as the "volume subjected to a stress amplitude above the 90 % of the maximum applied stress amplitude", i.e., the "risk-volume" or "V_{90}", according to the definition provided in Murakami.[7] Accordingly, for the same material, dog-bone specimens have been designed in order to have a risk-volume larger than that of the hourglass specimens.

The specimen geometries have been defined through finite element analyses (FEAs). A modal analysis has been carried out with the commercial software Ansys, by considering a specimen model discretized with 3D-20 nodes solid elements. The input elastic properties for each material have been experimentally assessed through the impulse excitation technique (IET) carried out on rectangular bars obtained from the plates used for cutting the specimens. The specimen lengths have been iteratively varied, with three main objectives. The first objective was to define a geometry ensuring that the first longitudinal resonance frequency of the specimen was close to 20 kHz (in the range [19.5–20.5] kHz, i.e., the working range of the ultrasonic fatigue testing machine). The second objective was to ensure that the required stress amplitude range at the specimen center could be applied, given the range of displacement amplitude that can be exerted with the piezoelectric transducer. The third one was to limit the stress concentration due to diameter variation in hourglass and dog-bone specimens. In particular, the ratio between the maximum stress in the specimen and the maximum stress along the specimen axis[15] has been kept conservatively below the 2 % for the hourglass specimens and 3.5 % for the dog-bone specimens. Accordingly, a stress concentration factor below 1.04 can be considered acceptable and is equal, or smaller, than that of literature specimens subjected to the ultrasonic fatigue test.[16] The influence of the stress gradient due to the stress concentration and notch can be considered negligible and the designed geometries can be reliably used for assessing size-effect on the VHCF response. Among the specimen geometries that satisfy these design constraints, those that maximize the risk-volume in dog-bone specimens and that minimize the risk-volume in hourglass

specimens have been selected, with the main aim of extending the risk-volume range and more properly investigating the size-effect. The specimen thickness, an important parameter for investigating size-effect, has not been varied, because the specimens were cut from plates with thicknesses used for automotive applications, which is thus of interest for industries, and provided by the partners of the EU Fatigue4Light Project, within which the experimental activity has been carried out.

For each specimen geometry, the vicinity of vibration modes, i.e., bending and torsional, to the longitudinal mode at 20 kHz, has been also verified through FEA. The aim was to select specimen geometries with vibrational modes as far as possible from the longitudinal one at 20 kHz to avoid the presence of any spurious mode during the ultrasonic test. For all the tested specimens, bending and torsional modes have been verified to be outside the working range, 19.5–20.5 kHz, of the ultrasonic fatigue testing machine, thus not influencing the applied tension-compression axial stress.

Figure 1 shows the geometry of the tested specimens, whereas Table 2 provides details on the gauge diameter (D_h) of the tested hourglass specimens and of the gauge diameter (D_d), the gauge length (L) and the radius (r_{db}) of the dog-bone specimens, together with the risk-volume of each tested specimen. In the sixth column (risk-volume of dog-bone specimens), the ratio between the risk-volume of dog-bone specimens (V90, db) and of hourglass specimens (V90, h) is reported.

According to Table 2, the ratio between the risk-volume of dog-bone and hourglass specimens is above 3 for all the tested materials, reaching up to 6.8 for the 22MnB5 steel.

The width at the gauge section, moreover, has been increased from the hourglass and the dog-bone specimen. The designed geometries, therefore, allows for a proper assessment of the influence of the specimen size for the investigated materials.

FIG. 1 Geometry of the tested specimens: (*A*) hourglass and (*B*) dog-bone.

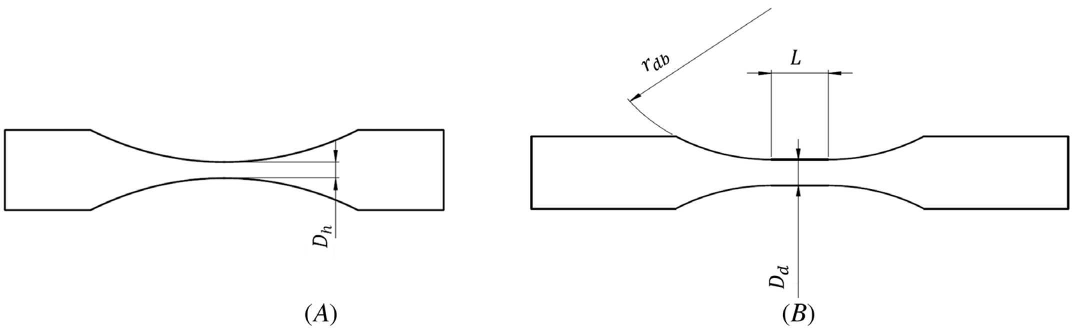

TABLE 2
Geometrical parameters and risk-volumes of the tested specimens

	Hourglass		Dogbone				
	D_h, mm	V_{90}, mm^3	D_d, mm	L, mm	r_{db}, mm	V_{90}, mm^3	$\frac{V_{90,db}}{V_{90,h}}$
AA6082, T6	4	72	5	10	31.4	391	5.4
HRCP800	3	79	5	10	30.4	265	3.4
HRCP980	2.9	76	5	10	30.4	265	3.5
AISI-410S	3	90	5.6	10	32.0	341	3.8
22MnB5	3	76	5.4	10	31.4	514	6.8

ULTRASONIC FATIGUE TESTING CONFIGURATION

The ultrasonic fatigue machines developed at the Politecnico di Torino have been used for the experimental tests. Fully reversed tension-compression tests have been performed at a loading frequency of 20 kHz up to failure or to 10^8 cycles (runout number of cycles). The testing systems, commonly used for testing specimens with circular cross-sections, have been adapted to test thin and flat specimens. A rigid connection between the horn and the specimen must be obtained to ensure the wave propagation and the required stress amplitude within the risk-volume. To this aim, the specimens are commonly bonded by the authors to the horn through an adhesive butt joint, which ensures a high-strength joint without the need of manufacturing a threaded hole in the horn and in the specimen. However, for the 2 mm thick aluminum alloy specimens, this connection was rather difficult. A keyseat-like hole with a depth of 2 mm has been manufactured at the horn end where the specimen was to be bonded. This facilitated the adhesively bonded connection between the horn and the specimen and prevented buckling-induced or bending stresses.

The applied stress amplitude at the specimen center has been verified with a strain gauge calibration, providing the correlation between the input voltage and the stress amplitude at the specimen center. Moreover, the displacement amplitude at the specimen free end has been continuously measured during the experimental tests with a laser displacement sensor.

The specimen self-heating has been kept under control during the experimental tests, with the temperature at the specimen center measured with an infrared sensor. Intermittent testing was carried out for those specimens and materials subject to a rapid temperature rise. In particular, during the pulse phase, the test was stopped if the measured temperature exceeded the maximum allowed value of 25°C, and automatically restarted when the measured temperature dropped below at least 23°C. A control system has been developed in the LabView environment to automatically manage the transition between the pulse phase and the cooling phase. Two vortex tubes have been also employed to limit the temperature increment and to speed up the cooling phase.

The tests were stopped when the specimen longitudinal resonance frequency fell outside the working range of the ultrasonic fatigue testing machine, i.e., below 19,500 Hz. Only 3 out of more than 100 tested specimens fractured (split into two halves) at the end of the test.

Figure 2 shows an image of a tested specimen bonded to the horn, together with the laser displacement sensor and the infrared temperature sensor for monitoring the displacement and the specimen temperature during the tests, respectively.

FIG. 2

Ultrasonic fatigue testing configuration.

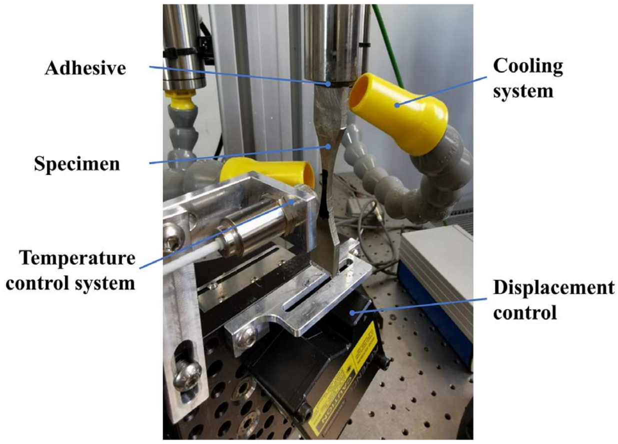

STATISTICAL MODEL FOR SIZE-EFFECTS IN VHCF

In order to properly model size-effects on the VHCF response of the tested flat specimens, a statistical model has been developed. Indeed, the International Standard ASTM E739-10, *Standard Practice for Statistical Analysis of Linear or Linearized Stress-Life (S-N) and Strain-Life (ε-N) Fatigue Data*, recommends the estimation of the median S-N curve with a linear regression of the data, according to the Basquin's model. The runout data are not considered in the analysis and the estimated parameters differ for the same material type if the specimen shape changes; i.e., for each investigated material one curve is estimated for the hourglass specimen and one curve for the dog-bone specimen, with the two curves characterized by different material parameters. As such, the design of a component whose loaded volume is even higher can be challenging.

In order to overcome these possible criticalities, a statistical analysis that can model size-effects in VHCF has been developed in Invernizzi et al.[12] The proposed methodology can be applied by considering the distribution of stress amplitude within the component volume, which can be easily assessed from the modal FEA carried out for the specimen design. The specimen volume can be discretized in uniformly stressed sub-elements; i.e., each specimen can be assumed as made of uniformly stressed sub-volumes, as shown in **figure 3**.

According to the Basquin's law, the larger the applied stress amplitude in the sub-volume, the smaller the fatigue life of the sub-volume. Moreover, according to the weakest-link principle, the larger the sub-volume, the smaller the fatigue life.[11] By combining these two physical-based assumptions, large sub-volumes subjected to a high-stress amplitude are the most critical. Further assumptions are related to the statistical distribution of the fatigue life, which is considered to follow a Weibull distribution with characteristic life η depending on the applied stress amplitude, according to the Basquin's law, and constant shape parameter β. The probability of failure of a generic element with unit volume ($v = 1$) due to an applied stress amplitude equal to s_i can be expressed as the following:

$$P[Y|_{s=s_i,\,v=1} \le y] = F_{Y|_{s=s_i,\,v=1}}\left(y; s_{\mathrm{MAX}}, \frac{s_i}{s_{\mathrm{MAX}}}\right) \tag{1}$$

where Y is the random variable (rv) logarithm of the fatigue life, y is the determination of the rv Y, $F_{Y|_{s=s_i,\,v=1}}$ is the cumulative distribution function (cdf) of the fatigue life, and s_{MAX} is the maximum applied stress amplitude within the component volume. According to the weakest-link principle and by assuming a Weibull distribution for the fatigue life, the probability of failure of a component assumes the compact form reported in equation (2) (for details on the analytical passages, the reader is referred to Invernizzi et al.[12]):

$$F_{N_f|_{s=s_i,=1}}\left(n; s_{\mathrm{MAX}}, \frac{s_i}{s_{\mathrm{MAX}}}\right) = 1 - e^{-\left(\frac{n}{\eta_i}\right)^{\beta}} \tag{2}$$

where n is the number of cycles to failure and η_i the scale parameters, function of the applied stress ratios ($s_{\mathrm{ratio},i} = \frac{s_i}{s_{\mathrm{MAX}}}$); i.e., the ratio between the applied stress s_i and the maximum stress within the component, with the following expression:

FIG. 3

Example of uniformly stressed sub-volumes (Aluminum specimens) obtained with a modal FEA.

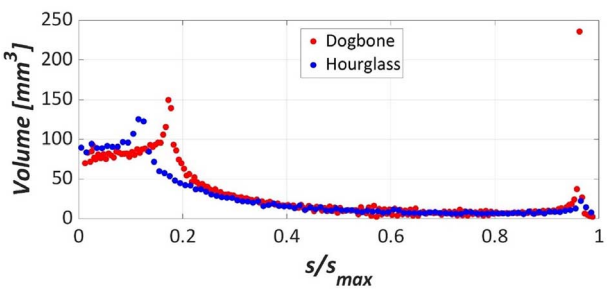

$$\eta_i = b \cdot s_{\mathrm{MAX}}^k \cdot \left(\frac{s_i}{s_{\mathrm{MAX}}}\right)^k = b \cdot s_{\mathrm{MAX}}^k \cdot s_{\mathrm{ratio},i}^k \tag{3}$$

where b and k are two constant parameters to be estimated from the experimental data.

By substituting equation (3) in equation (2) and with some passages, an equivalent volume can be defined, as follows:

$$v_{\mathrm{eq}} = \sum_{i=1}^{n_s} v_i s_{\mathrm{ratio},i}^{-\beta k} \tag{4}$$

Similarly, an equivalent scale factor η_{eq} can be defined as follows:

$$\eta_{\mathrm{eq}} = b \cdot v_{\mathrm{eq}}^{-1/\beta} \cdot s_{\mathrm{MAX}}^k \tag{5}$$

According to equation (5), the scale factor η_{eq} is a function of v_{eq}, which is, in turn, a function of the stress distribution, allowing to account for size-effects. The final general form of the probability of failure is reported in equation (6):

$$F_{N_f}(n; s_{\mathrm{MAX}}) = 1 - e^{-\left(\frac{n}{\eta_{\mathrm{eq}}}\right)^{\beta}} \tag{6}$$

Equation (6) models the probability of failure of a component by considering the stress distribution within its volume. Differently from Invernizzi et al.[12] (where four parameters must be estimated), equation (6) depends on three parameters, β, b and k, that must be estimated from the experimental data. With this approach, the distribution of the defect size, generally considered for modeling size-effect in VHCF,[7–9] is not necessary, simplifying the analysis of the experimental data.

Experimental Results

In this section, the experimental results are analyzed. In the section "Calibration Results," the results of the gage calibration carried out on thin aluminum specimens have been analyzed. In the "Analysis of Size-Effect in VHCF" section, the experimental data are analyzed. In the "Discussion" section, the influence of size-effects on the VHCF response of flat specimens is discussed and the experimental results are compared with literature data.

CALIBRATION RESULTS

Aluminum hourglass specimens are characterized by the smallest thickness among the tested specimens. For these thin specimens, the occurrence of buckling-induced stresses during the compression phase has been experimentally verified with strain gauges. One micro strain gauge (HBM 1-LY11-0.3/120) has been bonded at the specimen center on one specimen side and another strain gauge (HBM 1-LY11-0.3/120) in the same position on the opposite side, as shown in **figure 4A**. Each strain gauge has been connected in a quarter bridge configuration and the acquired signal has been properly amplified with a high-speed data acquisition device (sample rate of $3 \cdot 10^5$ Hz). During the calibration, the input voltage provided to the piezoelectric transducer has been varied in the range 1.1;1.5 V, avoiding a rise of the temperature at the specimen center that could affect the stress measurement and damage the micro strain gauge. From the acquired signal, the stress amplitude at the specimen center has been obtained through trigonometric interpolation and by considering the elastic modulus of the aluminum alloy assessed with the IET. **Figure 4B** plots stress amplitude acquired by the strain gauges with respect to the input voltage.

FIG. 4 Strain gauge validation on thin (2 mm thickness) Al alloy specimens: (*A*) specimen and micro strain gauges and (*B*) applied stress amplitude with respect to input voltage.

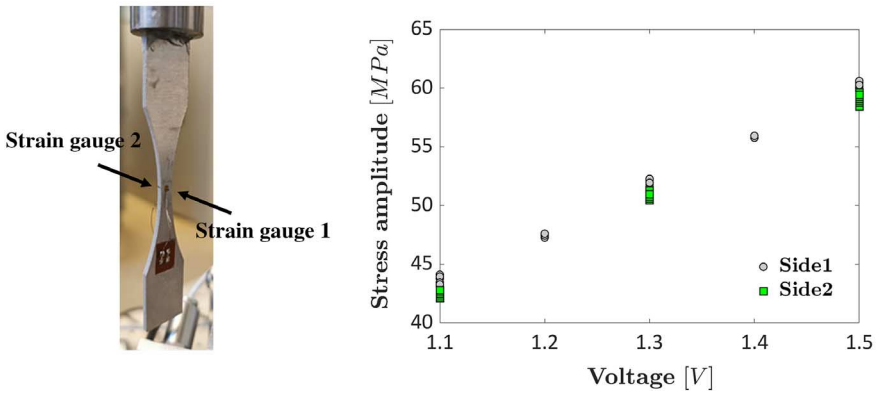

(*A*) (*B*)

According to figure 4*B*, the difference between the stress amplitude acquired by strain gauge attached to side 1 and strain gauge attached to side 2 is limited and can be mainly ascribed to errors in the strain gauge positioning. As expected, the experimental data acquired by gauges 1 and 2 follow the same linear trend and overlap for the same input voltage. This validation confirms that bending and buckling-induced stresses can be excluded for the thinnest tested specimens, and, accordingly, for the other tested specimens characterized by a larger thickness.

ANALYSIS OF SIZE-EFFECT IN VHCF

In this section, the experimental results have been analyzed with the proposed statistical model. The specimens that fractured at the end of the test have been observed with the optical microscope, but the initial defect was not visible. A surface crack originated the fatigue failure for the observed specimens and, reasonably, for the other specimens. The crack originated from the specimen surface for both hourglass and dog-bone specimens. Accordingly, a size-effect associated to the crack origin can be excluded. The maximum likelihood principle, which allows for the consideration of both failures and runout data, has been applied for the estimation of the material parameters of the developed statistical model. In particular, a Matlab script has been implemented to efficiently estimate these unknown parameters. The stress distribution within the specimens, i.e., the input of the model, has been obtained from the modal analysis carried out for the specimen design. Figure 5 shows the S-N plot of the tested AA 6082 T6 alloy. The estimated median and 0.01-th quantile P-S-N curve (99 % reliability, design curve in fig. 5) are plotted.

According to figure 5, the experimental data obtained by testing the hourglass specimens are above the data obtained through tests on dog-bone specimens. The scatter of experimental data is large, especially for hourglass specimens, with two failure data significantly below the other experimental failures. If the P-S-N curves are considered, the size-effects are evident, with the curves for hourglass specimens above the P-S-N curves for dog-bone specimens. For a number of cycles to failure of 10^8 cycles, the median fatigue strength estimated by considering the dog-bone specimens is about 8 % smaller than that estimated by considering the hourglass specimens.

Figure 6 shows the S-N plot of the tested HRCP800 steel. The median and the 0.01-th quantile P-S-N curves (99 % reliability, design curve in fig. 6) are also plotted.

According to figure 6, size-effects are evident, with the experimental data and the P-S-N curves for the hourglass specimens above experimental data and the P-S-N curve for dog-bone specimens. The experimental data obtained by testing dog-bone specimens show a larger scatter, with two experimental failures significantly

FIG. 5 S-N plot of the experimental data obtained by testing the AA 6082 T6 specimens and estimated median and 0.01-th quantile P-S-N curves.

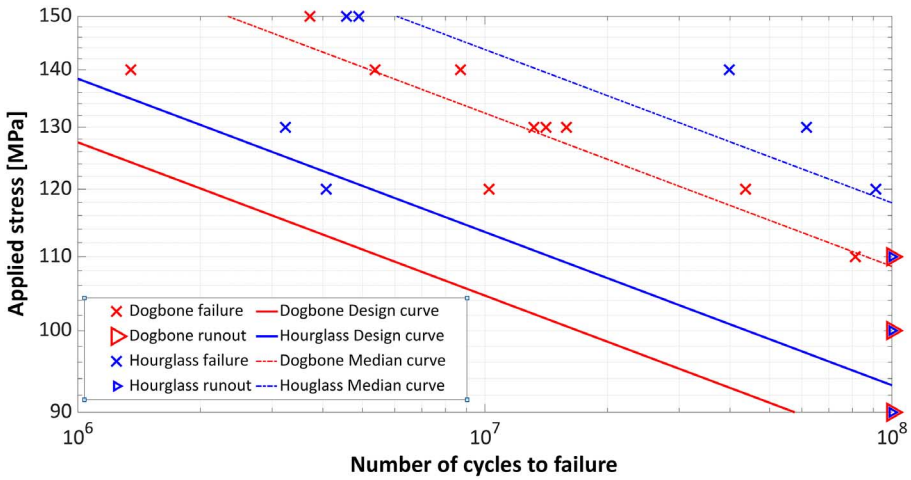

FIG. 6 S-N plot of the experimental data obtained by testing the HRCP800 specimens and estimated median and 0.01-th quantile P-S-N curves.

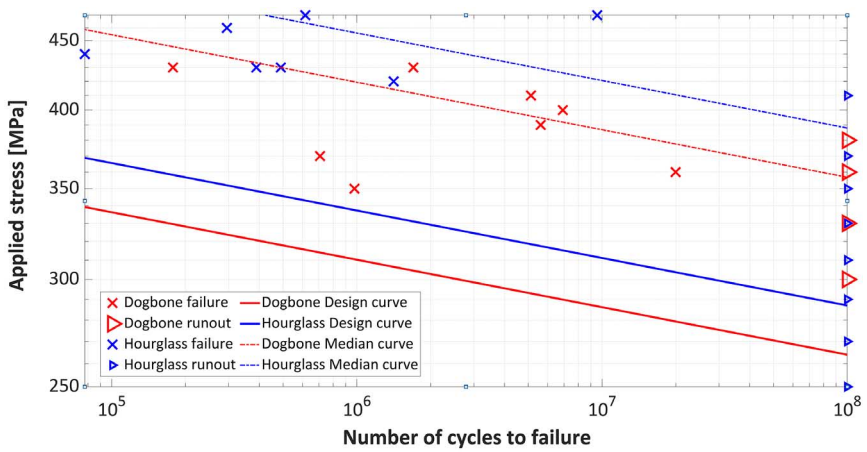

below the other failures. At 10^8 cycles to failure, the median fatigue strength estimated by considering the dog-bone specimens is 8 % smaller than that estimated with the hourglass specimens.

Figure 7 shows the S-N plot of the tested HRCP980 steel. The median and the 0.01-th quantile P-S-N curves (99 % reliability, design curve in **fig. 7**) are also plotted.

According to **figure 7**, experimental failures are mainly concentrated below 10^6 cycles, with only one failure at $2 \cdot 10^6$ cycles for the dog-bone specimens, and two failures above $4 \cdot 10^7$ cycles for the hourglass specimens. Size-effects are hidden by the larger scatter in the high cycle fatigue life region, whereas they are more evident in the VHCF life region. The P-S-N curves estimated by testing the two specimen geometries are closer with respect to the other investigated materials, with a 2 % fatigue strength reduction at 10^8 cycles (by considering the median curve).

Figure 8 shows the S-N plot of the tested AISI 410S steel. The median and the 0.01-th quantile P-S-N curves (99 % reliability, design curve in **fig. 8**) are also plotted.

FIG. 7 S-N plot of the experimental data obtained by testing the HRCP980 specimens and estimated median and 0.01-th quantile P-S-N curves.

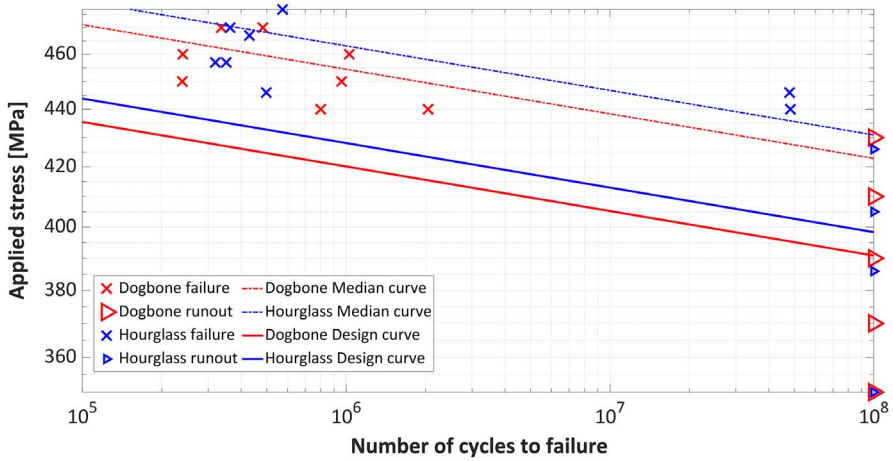

FIG. 8 S-N plot of the experimental data obtained by testing the AISI-410S specimens and estimated median and 0.01-th quantile P-S-N curve.

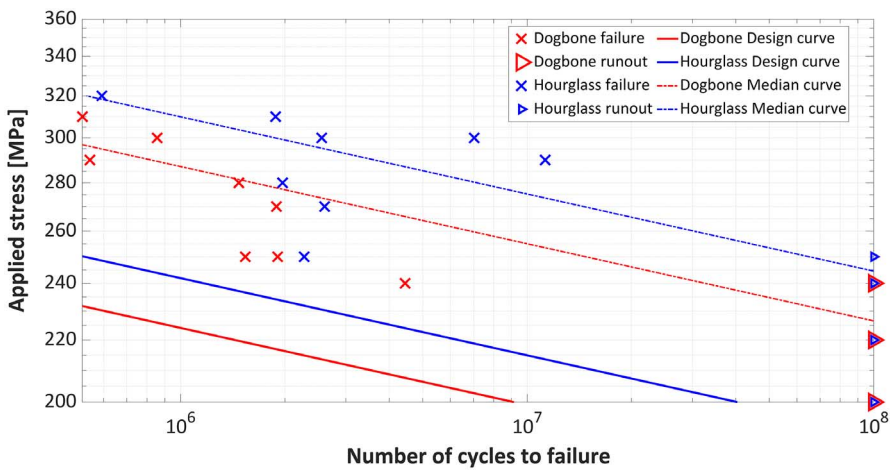

According to figure 8, the experimental data for the hourglass specimens are above the experimental data for the dog-bone specimens, with the difference being larger, close to 10^7 cycles. At 10^8 cycles to failure, the median fatigue strength estimated by considering the dog-bone specimens is 8 % smaller than that estimated with hourglass specimens.

Finally, figure 9 shows the S-N plot of the tested PHS 22MnB5 steel. The median curve and the 0.01-th quantile P-S-N curve (99 % reliability, design curve in fig. 9) are also plotted.

According to figure 9, most of the data obtained by testing the hourglass specimens are above the data obtained through tests on dog-bone specimens. Hourglass specimens show a large scatter, with one specimen failed below 10^6 cycles at 340 MPa, and one runout data. However, size-effects are evident, with the median fatigue strength at 10^8 cycles estimated by considering the dog-bone specimen reduced by about 10 %.

FIG. 9 S-N plot of the experimental data obtained by testing the PHS 22MnB5 specimens and estimated median and 0.01-th quantile P-S-N curves.

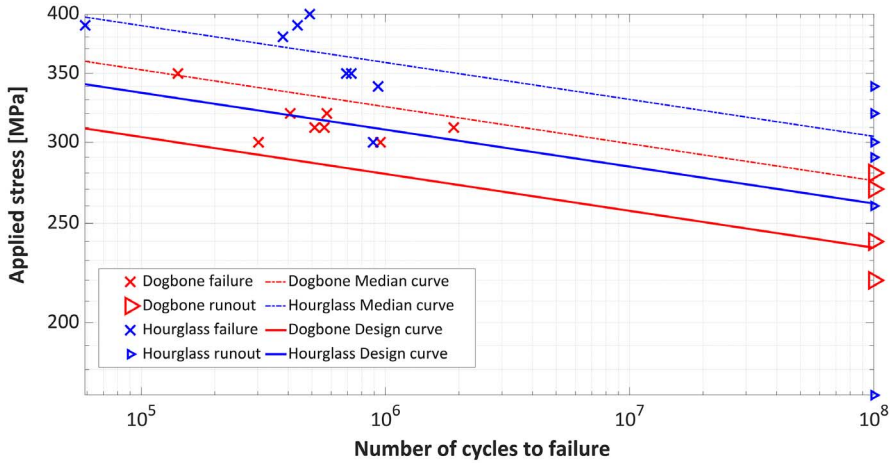

Discussion

For all the tested materials, the statistical model developed for the analysis of the experimental data can be reliably exploited for assessing size-effect in VHCF, with the stress distribution within the part required as the unique input parameter. The stress distribution within the part significantly influences the VHCF response and must be considered when size-effects are modeled. The proposed methodology, moreover, can also reliably model the experimental scatter. Indeed, apart from two failures, the 0.01-th quantile curves were found to be below the corresponding experimental failures, as expected. This analysis has also highlighted the importance of considering the size-effect and the experimental scatter when the fatigue response is analyzed. For example, 4 out of 8 failures in dog-bone 22MnB5 steel specimens are above the 0.01-th quantile curve estimated with the hourglass specimens. On the other hand, the 0.01-th quantile curve estimated by considering the dog-bone specimens is reliably below all the experimental failures, ensuring a conservative safety margin.

Table 3 summarizes the fatigue strength reduction at 10^8 cycles. The ratio between the risk-volume of the dog-bone and hourglass specimens ($V_{90,\text{dogbone}}/V_{90,\text{hourglass}}$) and the percentage fatigue strength reduction $((s_{\text{hourglass}} - s_{\text{dogbone}})/s_{\text{hourglass}}$, with s being the fatigue strength at 10^8 cycles as reported in columns 1 and 2, respectively.

According to Table 3, size-effects are significant for all the tested materials. Because two types of materials, aluminum and steel with four different characteristics, have been tested, it can be reliably concluded that size-effects significantly affect the VHCF response of flat specimens. For the AA6082 T6, HRCP800, AISI 410S, and 22MnB5 materials, the fatigue strength reduction is in the range [8:10]% for risk-volume increments

TABLE 3
Summary of size-effect for the investigated materials

	$V_{90,\text{dogbone}}/V_{90,\text{hourglass}}$	$(s_{\text{hourglass}} - s_{\text{dogbone}})/s_{\text{hourglass}}$
AA6082, T6	5.4	8 %
HRCP800	3.4	8 %
HRCP980	3.5	2 %
AISI-410S	3.8	8 %
22MnB5	6.8	9 %

in the range [3:7]. On the other hand, for a risk-volume increment in the same range, the VHCF reduction is about 2 % for the HRCP980. Accordingly, for the HRCP800 and HRCP980 steel specimens, with hourglass and dog-bone specimens characterized by the same risk-volumes and the same stress distribution, different fatigue strength variations have been found (2 % and 8 %). On the other hand, the same fatigue strength reduction has been found for specimens with different risk-volume variations and stress distributions (AA6082 T6, HRCP800, AISI 410S, and 22MnB5).

The results obtained in the present paper can be compared with literature results on size-effect in VHCF, even if specific tests on the same alloys with similar risk-volumes have been not carried out in the literature. All the fatigue failures have been found to originate from the specimen surface for the investigated materials, whereas specimens tested in the literature generally failed from internal defects.[17] This experimental difference can be explained by considering that the runout number of cycles to failure has been set to 10^8 cycles in the present paper, whereas it is generally above 10^9 cycles in literature papers.[17] The number of specimens which failed above 10^7 cycles is therefore larger in the literature, where internal defects have a dominant effect. Moreover, surface failures have been also found in the literature, even for specimens tested in the VHCF life region. For example, in Invernizzi, Montagnoli, and Carpinteri,[16] size-effects on the VHCF response of an aluminum alloy has been investigated with tests up to failure up to 10^{10} cycles, and all the specimens failed from the surface, with the initial defect non-observable with the scanning electron microscope.

Size-effect, as investigated by testing flat specimens in the present paper, is smaller than that generally found in the literature. This can be justified by considering that the risk-volume increment for the tested specimens, between 3 and 7, is smaller than that considered in the literature (e.g., close to 10 in Tridello et al.[18,19] and above 10 in Furuya and Tridello, Paolino, and Rossetto[8,10]). Accordingly, size-effect can be reasonably expected to be smaller in the present paper, with a VHCF strength decrement in the range of 2–10 % in the present paper and even above 30 % in the literature. Moreover, according to Tridello,[18] size-effect can also increase with the number of cycles to failure, depending on the tested material and on its degree of purity. Size-effect has been investigated by comparing the VHCF strength decrement at 10^8 cycles in the present paper, and at larger number of cycles in the literature. It must be also noted that a limited size-effect can be also related to a high material purity, as highlighted in Tridello.[18]

This analysis provides important indications for the design of components,[17,20,21] because size-effect must be carefully accounted for when components with large volumes are to be designed, relying on experimental results obtained by testing small specimens. However, in agreement with the literature review in Tridello et al.,[17] the analyses carried out in the present paper suggest that a general rule for size-effects in VHCF for thin flat specimens cannot be found, being strongly dependent on the material. Experimental tests to investigate size-effect are therefore recommended for materials to be employed in critical structural applications and prone to failures in the VHCF life region.

Conclusions

In the present paper, the influence of size-effects on the VHCF of flat specimens with thicknesses up to 6 mm has been experimentally verified. Fully reversed ultrasonic fatigue tests (loading frequency 20 kHz) have been carried out on one aluminum alloy (AA6082, T6) and 4 types of steel (HRCP800, HRCP980, AISI 410S, and 22MnB5) used in the automotive industry. Hourglass and dog-bone specimens with larger risk-volumes have been tested in order to investigate the size-effect on the VHCF response of flat specimens. The experimental results have been analyzed with a model developed by the authors that allows to assess the variation of the fatigue strength and of the probabilistic S-N curves with the specimen size, based on the stress distribution within the specimens and on the weakest-link principle.

The experimental results proved that size-effects strongly influence the VHCF response of flat specimens. For risk-volume increment ratios between 3 and 7, the fatigue strength decrement at 10^8 cycles for hourglass and dog-bone specimens was in the range of 8–10 % for the AA6082 T6 (aluminum alloy), HRCP800, AISI 410S, and

22MnB5 steels, whereas it is about 2 % for the HRCP980 steel. Moreover, for the different risk-volume ratios and, accordingly, stress distributions, between hourglass and dog-bone specimens (AA6082 T6, HRCP800, AISI 410S- and 22MnB5), the same fatigue strength reduction at 10^8 cycles has been experimentally found. Literature results have demonstrated that size-effect is strongly material dependent. The results obtained in the present paper have further confirmed this experimental evidence, with the VHCF decrement varying significantly even for steels with similar material properties and risk-volumes (e.g., 2 % and 8 % VHCF decrement at 10^8 cycles for the HRCP980 and the HRCP800, respectively). Moreover, failures originated in the specimen surface, whereas internal defects are mainly at the origin of the fatigue failures in literature results. This experimental evidence can suggest that also the crack origin can affect size-effect in VHCF, but more investigations are required to confirm this result. To conclude, the results obtained in the present paper further confirm that a general rule for size-effect in VHCF cannot be found even for flat specimens, because size-effects are strongly material dependent. Moreover, experimental tests are recommended to investigate the VHCF decrement with the specimen size of materials to be used for critical applications prone to VHCF failures, to guarantee a safe design. The proposed model proved effective in analyzing the experimental results obtained by testing specimens with different sizes and to analyze size-effect in VHCF, and it does not require the size of the defect at the origin of the fatigue failure, which is generally not available, especially if the crack originates from the specimen surface. Indeed, it has reliably modeled the P-S-N curve variation with the specimen size and large experimental scatter, further proving the effectiveness of this approach based on the stress distribution within the part.

ACKNOWLEDGMENTS

The research carried out in the paper has received funding from the European Union's Horizon 2020 innovation action program under grant agreement No. 101006844 – Fatigue4Light project.

References

1. C. Bathias and P. C. Paris, eds., *Gigacycle Fatigue in Mechanical Practice*, 1st ed. (New York: CRC Press, 2005).
2. C. Bathias, "Gigacycle Fatigue Properties of Bearing Steels," *Journal of ASTM International* 7, no. 4 (April 2010): 1–13, https://doi.org/10.1520/JAI102712
3. Q. Y. Wang, T. Lib, and X. G. Zenga, "Gigacycle Fatigue Behavior of High Strength Aluminum Alloys," *Procedia Engineering* 2, no. 1 (April 2010): 65–70, https://doi.org/10.1016/j.proeng.2010.03.007
4. J.-M. Zhang, L.-K. Ji, D.-J. Bao, Y.-R. Feng, S.-X. Li, and Y.-Q. Weng, "Gigacycle Fatigue Behavior of 1800 MPa Grade High Strength Spring Steel for Automobile Lightweight," *Journal of Iron and Steel Research, International* 21, no. 6 (June 2014): 614–618, https://doi.org/10.1016/S1006-706X(14)60095-9
5. E. Bayraktar, I. M. Garcias, and C. Bathias, "Failure Mechanisms of Automotive Metallic Alloys in Very High Cycle Fatigue Range," *International Journal of Fatigue* 28, no. 11 (November 2006): 1590–1602, https://doi.org/10.1016/j.ijfatigue.2005.09.019
6. M. Fitzka, B. Pennings, U. Karr, B. Schönbauer, R. Schuller, M.-D. Tran, and H. Mayer, "Influence of Cycling Frequency and Testing Volume on the VHCF Properties of 18Ni Maraging Steel," *Engineering Fracture Mechanics* 216 (July 2019): 106525, https://doi.org/10.1016/j.engfracmech.2019.106525
7. Y. Murakami, *Metal Fatigue: Effects of Small Defects and Nonmetallic Inclusions*, 1st ed. (Oxford: Elsevier Science, 2002).
8. Y. Furuya, "Notable Size Effects on Very High Cycle Fatigue Properties of High-Strength Steel," *Materials Science and Engineering: A* 528, no. 15 (June 2011): 5234–5240, https://doi.org/10.1016/j.msea.2011.03.082
9. D. S. Paolino, A. Tridello, G. Chiandussi, and M. Rossetto, "S-N Curves in the Very-High-Cycle Fatigue Regime: Statistical Modeling Based on the Hydrogen Embrittlement Consideration," *Fatigue & Fracture of Engineering Materials & Structures* 39, no. 11 (November 2016): 1319–1336, https://doi.org/10.1111/ffe.12431
10. A. Tridello, D. S. Paolino, and M. Rossetto, "Ultrasonic VHCF Tests on Very Large Specimens with Risk-Volume Up to 5000 mm^3," *Applied Sciences* 10, no. 7 (April 2020): 2210, https://doi.org/10.3390/app10072210
11. D. S. Paolino, "Very High Cycle Fatigue Life and Critical Defect Size: Modeling of Statistical Size Effects," *Fatigue & Fracture of Engineering Materials & Structures* 44, no. 5 (May 2021): 1209–1224, https://doi.org/10.1111/ffe.13424
12. S. Invernizzi, D. S. Paolino, F. Montagnoli, A. Tridello, and A. Carpinteri, "Comparison between Fractal and Statistical Approaches to Model Size Effects in VHCF," *Metals* 12, no. 9 (September 2022): 1499, https://doi.org/10.3390/met12091499
13. M. Duchet, J. Haouas, E. Gibeau, F. Pechenot, C. Honecker, R. Muniera, and B. Weber, "Improvement of the Fatigue Strength of Welds for Lightweight Chassis Application Made of Advanced High Strength Steels," *Procedia Structural Integrity* 19 (2019): 585–594, https://doi.org/10.1016/j.prostr.2019.12.063

14. S. Parareda, D. Casellas, D. Frómeta, M. Martínez, A. Lara, A. Barrero, and J. Pujante, "Fatigue Resistance of Press Hardened 22MnB5 Steels," *International Journal of Fatigue* 130 (January 2020): 105262, https://doi.org/10.1016/j.ijfatigue.2019.105262
15. D. S. Paolino, A. Tridello, G. Chiandussi, and M. Rossetto, "On Specimen Design for Size Effect Evaluation in Ultrasonic Gigacycle Fatigue Testing," *Fatigue & Fracture of Engineering Materials & Structures* 37, no. 5 (May 2014): 570–579, https://doi.org/10.1111/ffe.12149
16. S. Invernizzi, F. Montagnoli, and A. Carpinteri, "Experimental Evidence of Specimen-Size Effects on EN-AW6082 Aluminum Alloy in VHCF Regime," *Applied Sciences* 11, no. 9 (May 2021): 4272, https://doi.org/10.3390/app11094272
17. A. Tridello, C. Boursier Niutta, F. Berto, and D. S. Paolino, "Size-Effect in Very High Cycle Fatigue: A Review," *International Journal of Fatigue* 153 (December 2021): 106462, https://doi.org/10.1016/j.ijfatigue.2021.106462
18. A. Tridello, "VHCF Response of Two AISI H13 Steels: Effect of Manufacturing Process and Size-Effect," *Metals* 9, no. 2 (February 2019): 133, https://doi.org/10.3390/met9020133
19. A. Tridello, J. Fiocchi, C. A. Biffi, M. Rossetto, A. Tuissi, and D. S. Paolino, "Size-Effects Affecting the Fatigue Response up to 10^9 Cycles (VHCF) of SLM AlSi10Mg Specimens Produced in Horizontal and Vertical Directions," *International Journal of Fatigue* 160 (July 2022): 106825, https://doi.org/10.1016/j.ijfatigue.2022.106825
20. J. Paulo Davim, ed., *Modern Mechanical Engineering: Research, Development and Education*, 1st ed. (Berlin: Springer Berlin, Heidelberg, 2014), https://doi.org/10.1007/978-3-642-45176-8
21. J. Paulo Davim, ed., *Introduction to Mechanical Engineering*, 1st ed. (Cham, Switzerland: Springer Cham, 2018), https://doi.org/10.1007/978-3-319-78488-5